Cell Reports
Physical Science

CellPress
OPEN ACCESS

Article

Uncertainty and statistics of dislocation-precipitate interactions on creep resistance

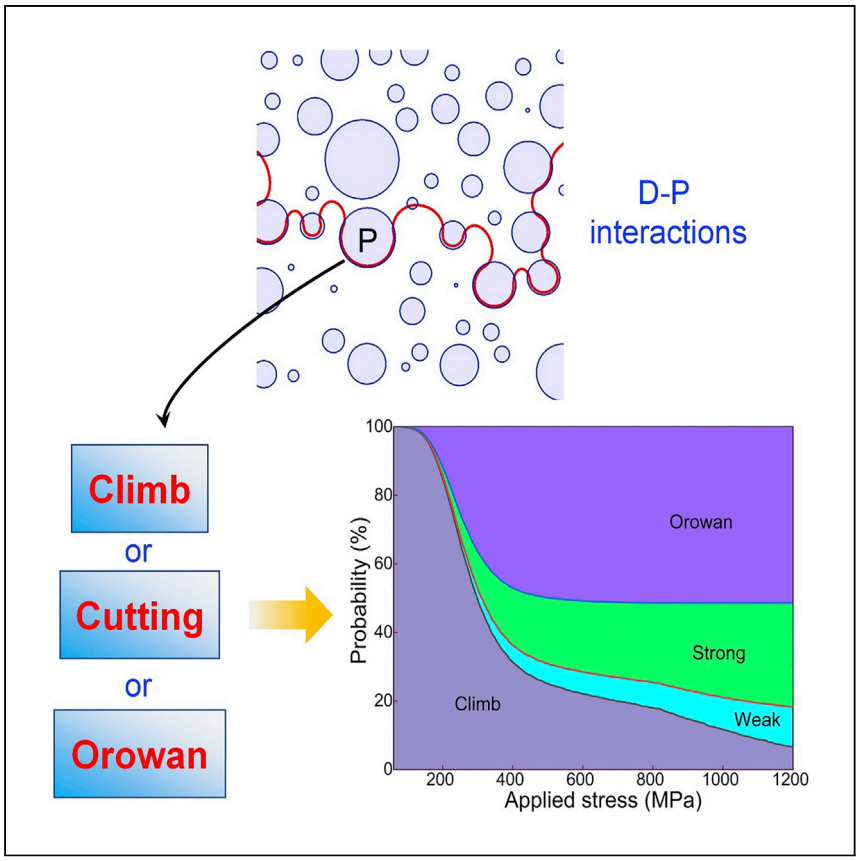

Considering the coexistence and uncertainty of climb, cutting, and Orowan mechanisms during creep processes, Li et al. develop a creep model coupling precipitate-spatial and precipitate-size lognormal distribution to predict accurately creep rate. This finding provides insights to design high-performance alloys under complex service environments.

Li Li, Feng Liu, Liming Tan, Qihong Fang, Peter K. Liaw, Jia Li

fangqh1327@hnu.edu.cn (Q.F.)
lijia123@hnu.edu.cn (J.L.)

Highlights

The model accounts for three-dimensional configuration of precipitates

The flaw of typical models with several-orders-of-magnitude deviations has been made up

The stress-controlled transformation of multiple creep mechanisms is revealed

The weighting of creep-resistance contributions from various mechanisms is evaluated

Li et al., Cell Reports Physical Science 3, 100704
January 19, 2022
https://doi.org/10.1016/j.xcrp.2021.100704

Cell Reports
Physical Science

CellPress
OPEN ACCESS

Article

Uncertainty and statistics of dislocation-precipitate interactions on creep resistance

Li Li,[1] Feng Liu,[2] Liming Tan,[2] Qihong Fang,[1,4,*] Peter K. Liaw,[3] and Jia Li[1,*]

SUMMARY

To meet the 30,000-h design lifetime of a typical turbine disc, understanding of long-term creep behavior is critical to prevent premature structural failure. The existing creep-life predictions often belittle the importance of multiple dislocation-precipitate interactions, resulting in several-orders-of-magnitude deviations in comparison with experiments. Herein, our experimental observation shows precipitate spatial distribution to yield uncertainty of dislocation-precipitate interactions and precipitate-size lognormal distribution to cause coexistence of climb, cutting, and Orowan mechanisms. Accounting for this physical process, we establish a unified model without adjustment parameters for predicting the stress-sensitive creep rate in precipitate-strengthened alloys. The predicted creep rates show agreement with experimental data, which makes up for the flaw of typical classic models with great deviations. Moreover, the present work reveals the stress-controlled transformation of multiple creep mechanisms and evaluates their weighting of creep-resistance contributions. Thus, our model provides insights for accurate design of high-strength and high-creep-resistant alloys under complex service environments.

INTRODUCTION

High-temperature alloys are currently significant structural materials for service in the aerospace and energy fields. For example, nickel-based superalloys have been widely used in aerospace propulsion and hotspot components in industrial gas turbine generators, such as combustors and turbine casings.[1,2] Advances in the turbine-engine performance, durability, and reliability, especially the thrust-to-weight ratio, have been closely tied to their high-temperature behavior.[3,4] After decades of development, superalloys exhibit excellent creep performance—that is, low plastic deformation under long-term high-temperature loads.[5,6] In-depth understanding of creep mechanisms and predictions of creep lifetime are the keys to developing advanced high-temperature alloys for meeting extreme service environment applications. The predicted results from existing creep models were typically insightful and illustrative. Meanwhile, the creep rate exhibited significant deviation between the experiment and prediction. In order to further elevate the prediction accuracy of creep rates and design high-temperature alloys with great creep resistance, a unified model for the stress-sensitive creep rate in precipitate-strengthened alloys is established by considering the uncertainty of dislocation-precipitate (D-P) interactions and the coexistence of climb, cutting, and Orowan creep mechanisms.

The D-P interactions are well known to control the high-temperature performance.[7–12] Recently, some high-performance precipitate-hardening alloys, such as high-entropy

[1]State Key Laboratory of Advanced Design and Manufacturing for Vehicle Body, College of Mechanical and Vehicle Engineering, Hunan University, Changsha 410082, PR China

[2]State Key Laboratory of Powder Metallurgy, Central South University, Changsha 410083, PR China

[3]Department of Materials Science and Engineering, The University of Tennessee, Knoxville, TN 37996, USA

[4]Lead contact

*Correspondence: fangqh1327@hnu.edu.cn (Q.F.), lijia123@hnu.edu.cn (J.L.)

https://doi.org/10.1016/j.xcrp.2021.100704

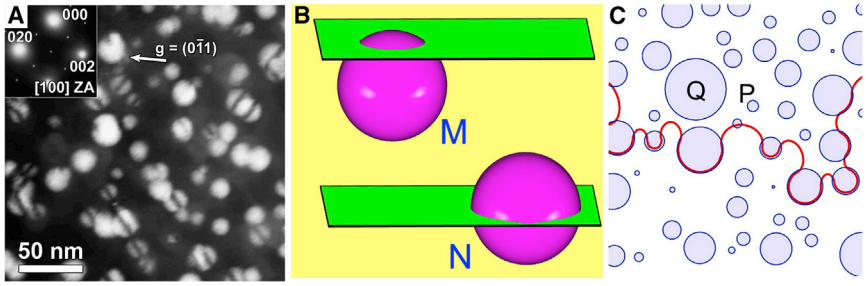

Figure 1. Schematic diagram of interaction between dislocations and three-dimensional precipitates

(A) Transmission electron microscope (TEM) micrograph of various D-P interactions.[21]

(B) A schematic illustration of D-P interactions by considering the relative position of the slip plane with respect to the position of three-dimensional precipitates with the same size.

(C) Typical static dislocation configuration during the dislocation-bypassing precipitates.

alloys and Mg alloys, were also designed by the spinodal decomposition, which is driven from the complex D-P interactions.[13,14] The creep resistance has been studied extensively by the existing model, assuming that dislocations pass through the equivalent-sized precipitate at a constant slip plane in the context of the climb or Orowan theory.[12,15–17] However, the existing creep models considered neither the precipitate-spatial distribution nor the precipitate-size statistical distribution (Figure 1). Thus, the early theoretical work was not consistent with the experimental observation,[18–21] and this trend is at the expense of huge deviations between the calculation and experiment for the creep rate. Clearly, it is necessary to clarify the reasonable contribution of the precipitate to creep resistance by considering the spatial and statistical distributions of precipitates.

As is well known, the dislocation-cutting mechanism is significant, especially for materials with nanoscale precipitates, which is universally proved by the experiments.[5,21] Based on the strengthening theory, the maximum precipitate strengthening occurs when the dislocation bypasses the precipitate by means of a cutting mechanism.[5] However, this important physical phenomenon during the creep process was neglected for a long time, resulting in the inaccurate assessment of the creep lifetime.[5] The creep experiments clearly suggest that the climb, cutting, and Orowan mechanisms concurrently take place, owning to two important factors: (1) the precipitate spatial distribution and (2) the precipitate-size statistical distribution.[21] Hence, considering the coexistence of multiple creep mechanisms, a unified statistical model is established to predict accurately the creep rates of precipitate-strengthened alloys.

RESULTS

Precipitate spatial distribution

It is generally assumed that the operative mechanism is determined by the average precipitate size, and the dislocation always interacts with the precipitate on the centered plane of a precipitate.[5,12,15–17] However, this feature is virtually not the true physical case. The slip plane of a dislocation is fixed within the material, but the precipitate is randomly distributed, as shown in Figure 1B. Therefore, even if the size of precipitates at different spatial positions is the same, there would be different dislocation-bypass mechanisms (Figure 1B). For example, the means of the dislocation bypassing a precipitate, "*M*," is the climb or cutting mechanism owing to the deviation between the dislocation slip plane and the central plane of the precipitate (Figure 1B). On the contrary, for the same-sized precipitate, "*N*," the operative mechanism is the Orowan mechanism (Figure 1B). Thus, the

precipitate spatial distribution yields the uncertainty of D-P-interaction mechanisms. In particular, for alloys with the large-size precipitate, the threshold stress is contributed to by the probability-dependent dislocation-bypassing process, including the climb, cutting, and Orowan mechanisms.

Here, considering the probability-dependent precipitate-bypassing mechanism, the effective critical resolved shear stress (CRSS) of creep resistance can be expressed as

$$\tau_{weak}^{new}(r) = p_0(r)\tau_{\text{climb}} + \int_0^r p_1(r)\tau_{weak}(r)dr \qquad r \le r_p$$

$$\tau_{strong}^{new}(r) = p_0(r)\tau_{\text{climb}} + \int_0^{r_p} p_1(r)\tau_{weak}(r)dr + \int_{r_p}^r p_2(r)\tau_{strong}(r)dr \qquad r_p < r < r_c$$

$$\tau_{orowan}^{new}(r) = p_0(r)\tau_{\text{climb}} + \int_0^{r_p} p_1(r)\tau_{weak}(r)dr + \int_{r_p}^{r_c} p_2(r)\tau_{strong}(r)dr + \int_{r_p}^r p_3(r)\tau_{Orowan}(r)dr \quad r_c \le r \qquad (1)$$

where τ_{climb} is CRSS of climb, and $\tau_{weak}(r)$, $\tau_{strong}(r)$, and $\tau_{Orowan}(r)$ represent CRSS of probability-dependent weak-pair coupling, strong-pair coupling, and Orowan mechanisms, respectively, which are derived in Note S1. $p_0(r)$ is acquired by the comparison between the applied shear stress and CRSSs. $p_1(r)$, $p_2(r)$, and $p_3(r)$ are expressed as $p_1(r) = 1 - (1-(r_p/r)^2)^{1/2}$, $p_2(r) = (1-(r_p/r)^2)^{1/2} - (1-(r_c/r)^2)^{1/2}$, and $p_3(r) = 1 - p_1(r) - p_2(r)$, respectively. Here, r_p is the critical size of a precipitate for the transformation from the weak-pair to strong-pair coupling, and r_c is the critical size for the transformation from the strong-pair coupling to Orowan mechanism. The detailed modeling and calculation in Equation (1) are described in Note S2. However, this important physical realistic process is neglected in the previous theoretical work, leading to the significant deviation in the predicted creep resistance.

Precipitate-size statistical distribution

It is assumed that "dislocations interact with the precipitate ensemble" can be equivalent to "dislocations interact with a precipitate with the mean size" in the previous work (Figure 1C).[5] However, this assumption is not physically realistic. In the present work, the precipitate sizes are dispersedly distributed, rather than using a single average size widely used in the previous model, as exhibited in Figure 1C (assuming that the average size of the precipitate is $\bar{r}$ in Figure 1C). The sizes of some precipitates may be less than $\bar{r}$, such as the precipitate "*P*" (or larger than $\bar{r}$, such as the precipitate "*Q*"), due to the size-statistical distribution demonstrated in the experiments.[18] The means of the dislocation-bypassing precipitates "*P*" and "*Q*" is highly likely to be different, thus leading to the occurrence of various creep mechanisms. Therefore, it is necessary to take the precipitate-size statistical distribution into account in the creep-strength theory for the accurate prediction of the creep life.

The experiment demonstrates that the law of the lognormal distribution can be employed to meet the precipitate size.[22] The probability density function of the precipitate-size distribution is given by $f(r) = \left(1/\sqrt{2\pi}\sigma r\right)\exp\left[-\left((\ln(r)-\mu)^2/2\sigma^2\right)\right]$, where μ and σ are the geometric mean value and the geometric standard deviation of $\ln(r)$, respectively.[23] Hence, considering the precipitate-size lognormal distribution, the climb, cutting, and Orowan mechanisms are simultaneous. The creep resistance from the precipitate is always contributed from the climb, weak-pair coupling, strong-pair coupling, and Orowan mechanisms:

$$\sigma_{thr}(r) = M\left(\int_0^{r_p} \tau_{weak}^{new}(r)f(r)dr + \int_{r_p}^{r_c} \tau_{strong}^{new}(r)f(r)dr + \int_{r_c}^{r_{max}} \tau_{orowan}^{new}(r)f(r)dr + \tau_{climb}\right) \quad (2)$$

where M is the Taylor orientation factor. $\tau_{weak}^{new}(r)$, $\tau_{strong}^{new}(r)$, and $\tau_{orowan}^{new}(r)$ come from Equation (1). r_{max} represents the maximum precipitate size. The detailed modeling and calculation process of the effective contributed stress for total precipitates is presented in Note S3. Therefore, the new equation of the threshold stress is proposed in Equation (2) by considering the physically realistic precipitate spatial distribution and precipitate-size statistical distribution.

The physical-based model because of the climb and Orowan mechanisms is widely developed for the prediction of the creep rate and its correlated creep lifetime.[24–26] Based on the previous work,[16] a unified equation of creep rates considering the precipitate spatial distribution and precipitate-size statistical distribution in the precipitate-strengthened alloys is proposed as

$$\dot{\varepsilon}_{sec} = \frac{2\tau_L b c_L N}{M}\left(\frac{\sigma_{app} - \sigma_{thr}(r)}{\alpha M G b}\right)^3 \quad (3)$$

where τ_L is the line tension of a dislocation, which is equal to $\tau_L = 0.5Gb^2$; b is the Burgers vector; c_L is a strain-hardening parameter; and N is the dislocation mobility, which is dependent on the stress and temperature in Note S4. M is the Taylor factor, σ_{app} is the applied stress, σ_{thr} is the threshold stress, α is the Taylor constant depending on the lattice structure, and G is the shear modulus. Here, the novel model of a threshold stress, $\sigma_{thr}(r)$, is dependent on various precipitate-bypass mechanisms, which rely on not only the precipitate size, but also the precipitate spatial and statistical distributions. It is necessary to emphasize that even though the precipitates are spherical in Figure 1, the present model is suitable for the other precipitates with irregular geometry. This is because the present model is based on two facts: (1) the slip plane of a dislocation is fixed within the material, but the precipitate is randomly distributed; and (2) the existence of a statistical distribution for precipitate size. These two facts also exist in the materials with cubic precipitates or other precipitates with irregular geometry. Therefore, it is believed that the present model is universal for precipitate-strengthened materials.

Creep-rate theory versus experiment

By coupling all the cases discussed in Figure 1 into the proposed unified statistical model, the effect of the applied stress on the creep behavior of high-temperature alloys can be evaluated in detail. Figure 2A exhibits the comparison between the experimental data and the predications from the classical model and present model in the MAR-M247 superalloy.[27] It is noted that the comparisons between the classic model and our work are all with the same parameters, other than the threshold stress. The threshold stresses are obtained from Equations S1–S4 in the classic model, while they are integrated into Equation (2) in the present work. As a result, the predicted creep rates from our model match the experimental results very well at various temperatures and stresses, compared to the classical model. In particular, the slope change with the increasing stress at the temperatures of 1,000°C and 950°C, indicating the operative creep-mechanism transformation from the climb mechanism to cutting/Orowan mechanism, is exactly taken into account. The degree of deviation in the predicted creep rate between the experiment and model is presented in Figure 2B. At 800°C, the value of the creep-rate deviation is, on average, less than 300% for the present model and up to 30,000% for the classical model. At

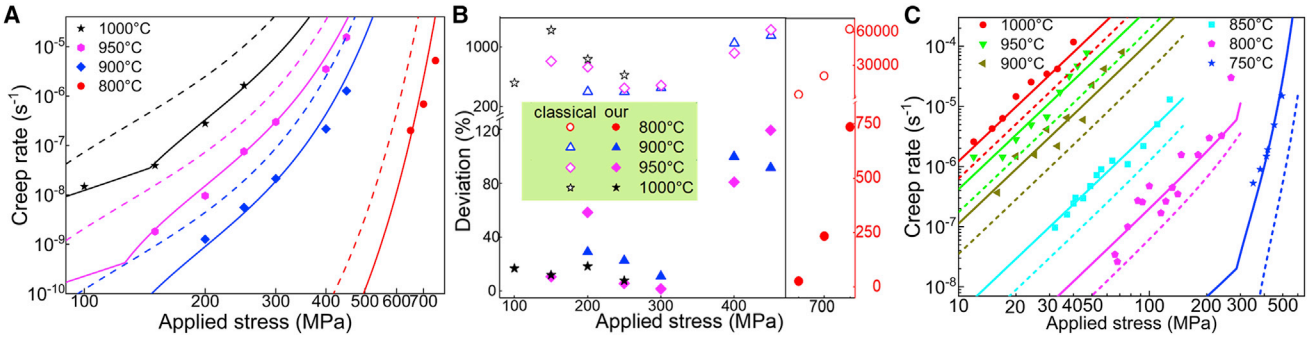

Figure 2. The comparisons between the previous experiments and theories

(A) The double logarithmic relationship between the creep rate and applied stress for the MAR-M247 superalloy, where the dots represent the experimental data, the solid lines denote the predicted results of the present model, and the dotted lines represent the results predicted by a classical model.[5,16]

(B) The deviation of the predicted creep rates among our model, a classical model, and experiments in the MAR-M247 superalloy. Here, the filled dots represent predictions from our model, and the hollow dots denote the predictions from a classical model. The deviations at 800°C correspond to the right axis. At 900, 950, and 1,000°C, they correspond to the left axis.

(C) The double logarithmic relationship between the creep rate and applied stress for the 718 superalloy. The dots represent the experimental data, the solid lines denote the predicted results of the present model, and the dotted lines represent the results predicted by a classical model.

900°C, it is, on average, less than 50% for our model, but larger than 600% for the classical model, revealing that the present model obviously outperforms the classical model. Hence, considering the precipitate spatial distribution and precipitate-size statistical distribution is necessary to predict the creep rate exactly and then achieve an accurate material design by reducing failure probability and enhancing reliability.

Figure 2C exhibits the comparison between the experimental data and the predications from the current model and the classical model of the 718 superalloy.[17] The results further prove that the present model can match the experimental results better, compared to the classical model, in a wide range of stresses and temperatures. When the applied stress is lower than 100 MPa, a nearly linear correlation between the applied stress and creep rate is presented in Figure 2C, in agreement with the classical power-law creep behavior. As the applied stress increases, the obvious variation of the slope also rises. The obvious transition of the creep rate can be observed in Figures 2A and 2C. This trend is derived from the transformation of the creep mechanisms from climb to cutting. When the applied stress is less than that of transition points, the climb mechanism dominates the creep mechanism. Moreover, a slight fluctuation could be observed at 750°C with increasing the applied stress, which is different from the linear correlation at the temperatures higher than 750°C (Figure 2C). This phenomenon is induced by the coexistence of multiple creep mechanisms due to the statistical distribution of precipitate sizes (Figure 1B). It is confirmed that the current method can also be applied to 718 superalloys with great success.

It is universally known that the service condition would strongly affect the creep performance and lifetime.[28] Here, our developed high-temperature superalloys are tested at 650°C/1,100 MPa and 750°C/690 MPa (Figure 3). Compared to the classical creep model, the accuracy of creep rates predicted from our model is significantly increased by about 10 times, on average (Figure 3A). The previous work overestimates the creep rate, especially at high stress levels, due to the underestimate of the threshold stress. The transmission electron microscopy (TEM) graphs also show that the climb, cutting, or Orowan mechanisms are concurrent at 650°C/1,100 MPa

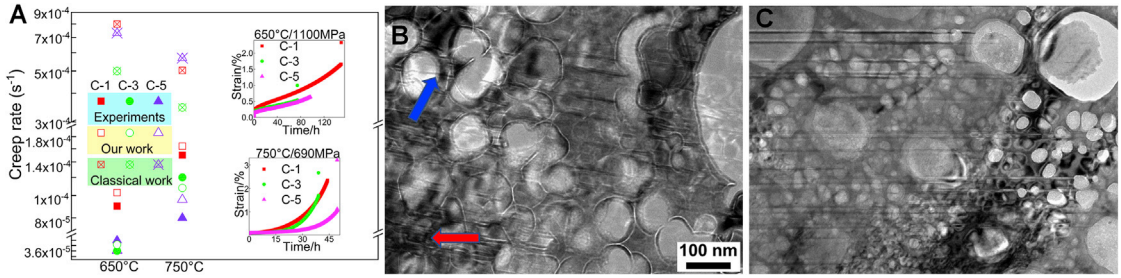

Figure 3. The comparisons between our experiments and theories and observation of multiple creep mechanisms

(A) The creep rate calculated by the classical model, the present model, and our experimental results. The solid points represent the experimental results, which are derived from the illustration in (A). Here, C-1, C-3, and C-5 are three types of nickel-based superalloys prepared by the powder metallurgy. The detailed preparation process, alloy composition, and microstructure characterization are presented in our experimental procedure.

(B) The TEM micrograph of the C-5 alloy after creep deformation under 650°C/1,100 MPa.

(C) The coexistence of climb, cutting, and Orowan mechanisms at 750°C/690 MPa.

The blue arrows in (B) and (C) indicate the dislocation-cutting mechanism. The red arrows in (B) and (C) denote the dislocation networks around the precipitate interface, which would bypass the precipitate through the climb or Orowan mechanisms.

and 750°C/690 MPa (Figures 3B and 3C), while only one mechanism was considered in the existing model.[5,16] Thereinto, for precipitates less than 52 nm, the cutting mechanism dominates creep strengths. For precipitates larger than 52 nm, the climb/Orowan mechanism governs the creep strength (Figure 3C), attributed to the criterion of the minimum critical threshold stress for various mechanisms.[25] Interestingly, the applied stress far exceeds the critical cutting stress, and the dislocation to mainly cut into precipitate is observed in Figure 3B. Hence, the creep deformation is dominated by the climb/Orowan mechanism at low stresses but by the cutting mechanism at high stresses. The phenomenon of the creep-mechanism transform with changing service conditions results in the coexisting multiple creep mechanisms, breaks the conventional assumption of a single creep mechanism, and brings the complexity of performance regulation.

DISCUSSION

In view of the coexistence of multiple creep mechanisms observed in experiments, how could we quantitatively determine the occurrence probability of different creep mechanisms, evaluate the contribution of the corresponding creep strength, and then accurately tune the microstructure to develop the high creep-resistant material? Figures 4A and 4B show the applied-stress-dependent creep mechanism. In region I, the applied stress is larger than the highest cutting stress at the precipitate size of R_1, resulting in the only occurrence of the cutting mechanism. In region II, the applied stress is not large enough for the dislocation to cut into a precipitate, leading to the occurrence of the climb mechanism. Considering the precipitate spatial distribution, the cutting mechanism is still present. In region III, the applied stress is larger than threshold stress at the precipitate size of R_2, resulting in the activated Orowan mechanism. The cutting and climb mechanisms are concomitant owing to the precipitate spatial distribution. Here, the applied-stress-controlled creep mechanisms are coupled into our model, which is contrary to the previous model considering only one mechanism under a given creep condition.[12,15–17,24,25]

In order to tune the size distribution of precipitates to enhance key mechanical properties, Figures 4C and 4D quantitatively describe the occurrence probability of different creep mechanisms and their contributions to the creep resistance with the changeable applied stress in a fixed temperature of 750°C. Here, although Figures 4C and 4D present for the C-5 superalloys at the test temperature of 750°C, they are representative for

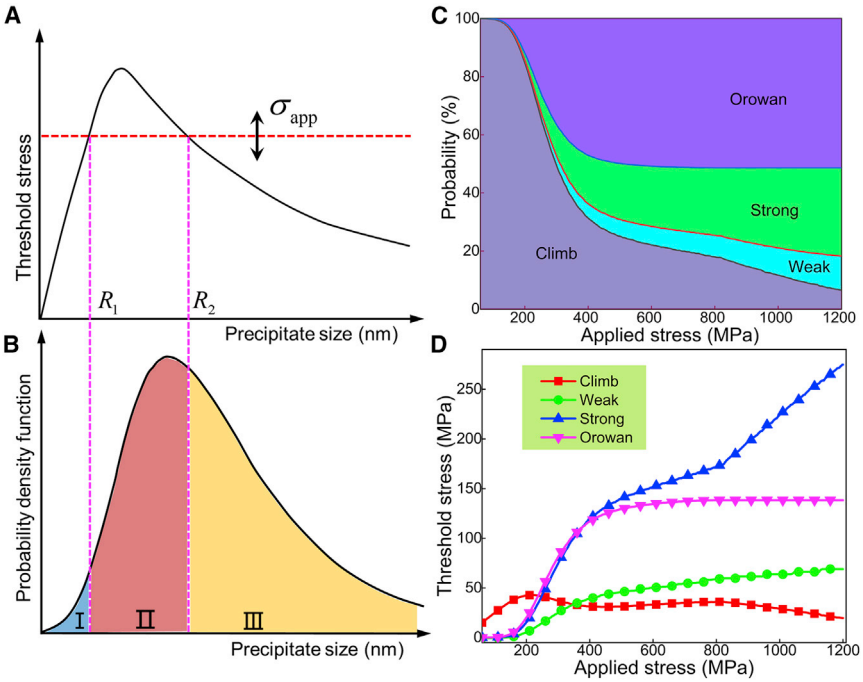

Figure 4. The calculation process for the probability and contributed creep resistance of various mechanisms

(A) The schematic illustration of the correlation between the applied stress and threshold stress derived from the precipitate.

(B) The distribution of various creep mechanisms, where three regions are divided according to the relationship of the applied stress and threshold stress. The two pink dotted lines would be close (far away) from each other with the increasing (decreasing) applied stress, which causes the change in regions, I, II, and III and controls the transformation of creep mechanisms.

(C) The occurrence probability of different creep mechanisms as a function of applied stress in C-5 superalloys at a fixed temperature of 750°C.

(D) The creep resistance contributed from various mechanisms in C-5 superalloys.

the other superalloys due to the relatively narrow fluctuation range of the compositions. Moreover, this model can be easily extended to the precipitate-hardened alloys with different microstructures and service conditions, using the corresponding classical creep formulas and material parameters, to quantitatively reveal the occurrence probability and contributions from various mechanisms. With the increasing applied stress, the cutting and Orowan mechanisms gradually substitute for the climb mechanism, which contributes the higher creep resistance. Here, at the low applied stress (σ_{app} < 200 MPa), the climb mechanism dominates the creep deformation and contributes the most to the creep resistance. When the applied stress increases to more than 200 MPa, the probability of the climb mechanism decreases sharply, resulting in an obvious transition point in Figures 2A and 2C. At intermediate stress (300 MPa < σ_{app} < 700 MPa), the strong-pair coupling produces an equal contribution to creep resistance, compared with the Orowan mechanism. At high stress (700 MPa < σ_{app}), the creep resistance is mainly contributed from the strong-pair coupling (Figure 4D). It is interesting to note that although the Orowan mechanism is more widely present, the cutting mechanism contributes higher creep resistance (Figures 4C and 4D). This new finding breaks the traditional cognition where the Orowan mechanism contributes to the most creep resistance.

Table 1. Nominal compositions of three superalloys in weight percent

	Co	Cr	Mo	W	Al	Ti	Ta	C	B	Zr	Ni
C-1	25.0	12.5	5	0	3.0	4.0	4.0	0.04	0.03	0.05	bal.
C-3	25.0	12.5	4.0	2.0	3.0	4.0	4.0	0.04	0.03	0.05	bal.
C-5	25.0	13.5	2.5	4.0	2.5	4.6	1.6	0.04	0.03	0.05	bal.

Considering the precipitate spatial distribution and precipitate-size lognormal distribution from the experimental observation, we have proposed a unified statistical model without adjustment parameters, and we achieve an accurate prediction of creep rates and creep resistance over a wide range of stresses and temperatures. The present work obtains the occurrence probability of various creep mechanisms with the increased applied stress and evaluates their weighting of contributions to creep resistance. The climb mechanism governs the creep resistance at low stresses, and the Orowan coupled with cutting mechanisms dominate it at high stresses, which challenges the conventional view that only the Orowan mechanism has a leading role in the existing model. Correspondingly, to enhance creep performance, this strategy should be considered in multimodal precipitate sizes: reducing the size of a precipitate larger than the critical size, r_c, at the intermediate stress and increasing the volume fraction of a precipitate less than r_c and larger than r_p at the high stress. The current work can provide new insights into the stress-dependent creep mechanism by considering the uncertainty of D-P interactions and assist the accurate design of ultra-strong creep-resistant alloys.

EXPERIMENTAL PROCEDURES

Resource availability

Lead contact

Further information and requests for resources and materials should be directed to and will be fulfilled by the lead contact, Qihong Fang (fangqh1327@hnu.edu.cn).

Materials availability

This study did not generate new unique reagents.

Data and code availability

All of the data reported in this article will be shared by the lead contact upon request.

Materials and methods

With nominal compositions listed at Table 1, three novel superalloys are prepared by powder metallurgy routes. Specifically, master alloys were first fabricated by vacuum induction melting (VIM), and then the powders within sizes of 150 μm were obtained by argon atomization and screening. Thereafter, the powders were consolidated by the hot extrusion at 1,130°C with an area reduction of 16:1. Finally, the billets were heat treated at subsolvus temperature of 1,100°C for 2 h and air cooled and aged at 750°C for 24 h.

The initial microstructures before creep are listed in Table 2. All the creep specimens were cut from the billets along the extrusion direction, and the creep tests were performed in conditions of 650°C/1,100 MPa and 750°C/690 MPa. The microstructure was observed by a Quanta 650 FEG field-emission scanning electron microscope (SEM). In addition, samples for TEM observations were sliced from creep samples beneath the fractured surface, and the slices were twin-jet electropolished in the corrosive reagent of 90% (volume percent) ethanol plus 10% perchloric acid at –25°C and 20 V. The TEM observation was conducted on

Table 2. Initial microstructures of three P/M superalloys after heat treatment

Alloy	Average grain size, μm	Secondary γ′		Tertiary γ′	
		Volume fraction, %	Equivalent diameter, nm	Volume fraction, %	Equivalent diameter, nm
C-1	2.7	36.6	307	15.0	60
C-3	5.4	37.1	300	15.6	64
C-5	4.2	32.5	270	16.7	74

a field-emission TEM Tecnai G2 F20 with a 200-kV-accelerating voltage to characterize the D-P interaction.

SUPPLEMENTAL INFORMATION

Supplemental information can be found online at https://doi.org/10.1016/j.xcrp.2021.100704.

ACKNOWLEDGMENTS

The authors deeply appreciate the support from Foundation for Innovative Research Groups of the National Natural Science Foundation of China (51621004), and the National Natural Science Foundation of China (12072109, 51871092, and 12172123). P.K.L. very much appreciates the support from the U.S. National Science Foundation (DMR-1611180 and 1809640).

AUTHOR CONTRIBUTIONS

L.L., Q.F., P.K.L., and J.L. conceived and designed this research. F.L. and L.T. conducted the experiments. L.L. and J.L. analyzed the data and built the model. All the authors contributed to manuscript preparation.

DECLARATION OF INTERESTS

The authors declare no competing interests.

Received: August 17, 2021
Revised: November 8, 2021
Accepted: December 3, 2021
Published: December 29, 2021

REFERENCES

1. Pollock, T.M. (2016). Alloy design for aircraft engines. Nat. Mater. *15*, 809–815.

2. Darling, K.A., Rajagopalan, M., Komarasamy, M., Bhatia, M.A., Hornbuckle, B.C., Mishra, R.S., and Solanki, K.N. (2016). Extreme creep resistance in a microstructurally stable nanocrystalline alloy. Nature *537*, 378–381.

3. Wu, X., Makineni, S.K., Liebscher, C.H., Dehm, G., Mianroodi, J.R., Shanthraj, P., and Gault, B. (2020). Unveiling the Re effect in Ni-based single crystal superalloys. Nat. Commun. *11*, 1–13.

4. Panwisawas, C., Tang, Y.T., and Reed, R.C. (2020). Metal 3D printing as a disruptive technology for superalloys. Nat. Commun. *11*, 2327.

5. Reed, R.C. (2008). The superalloys: fundamentals and applications (Cambridge University Press).

6. Castellanos, D.F., and Zaiser, M. (2018). Avalanche behavior in creep failure of disordered materials. Phys. Rev. Lett. *121*, 125501.

7. Yang, T., Zhao, Y.L., Tong, Y., Jiao, Z.B., Wei, J., Cai, J.X., Han, X.D., Chen, D., Hu, A., Kai, J.J., et al. (2018). Multicomponent intermetallic nanoparticles and superb mechanical behaviors of complex alloys. Science *362*, 933–937.

8. Jiao, Z.B., Luan, J.H., Miller, M.K., Chung, Y.W., and Liu, C.T. (2017). Co-precipitation of nanoscale particles in steels with ultra-high strength for a new era. Mater. Today *20*, 142–154.

9. Fu, Z., Jiang, L., Wardini, J.L., MacDonald, B.E., Wen, H., Xiong, W., Zhang, D., Zhou, Y., Rupert, T.J., Chen, W., and Lavernia, E.J. (2018). A high-entropy alloy with hierarchical nanoprecipitates and ultrahigh strength. Sci. Adv. *4*, eaat8712.

10. Cheng, T.L., and Wen, Y.H. (2021). Phase-field model of precipitation processes with coherency loss. NPJ Comput. Mater. *7*, 1–11.

11. Meher, S., Aagesen, L.K., Carroll, M.C., Pollock, T.M., and Carroll, L.J. (2018). The origin and stability of nanostructural hierarchy in crystalline solids. Sci. Adv. *4*, eaao6051.

12. Peng, S., Wei, Y., and Gao, H. (2020). Nanoscale precipitates as sustainable dislocation sources for enhanced ductility and high strength. Proc. Natl. Acad. Sci. USA *117*, 5204–5209.

13. Liang, Y.J., Wang, L., Wen, Y., Cheng, B., Wu, Q., Cao, T., Xiao, Q., Xue, Y., Sha, G., Wang, Y., et al. (2018). High-content ductile coherent nanoprecipitates achieve ultrastrong high-entropy alloys. Nat. Commun. *9*, 4063.

14. Xin, T., Zhao, Y., Mahjoub, R., Jiang, J., Yadav, A., Nomoto, K., Niu, R., Tang, S., Ji, F., Quadir, Z., et al. (2021). Ultrahigh specific strength in a magnesium alloy strengthened by spinodal decomposition. Sci. Adv. *7*, 3039.

15. Brown, L.M., and Ham, R. (1971). Strengthening Mechanisms in Crystals (Elsevier Publishing Company Ltd).

16. Kocks, U.F., Argon, A.S., and Ashby, M.F. (1975). Thermodynamics and kinetics of slip. Prog. Mater. Sci. *19*, 1–281.

17. Drexler, A., Fischersworring-Bunk, A., Oberwinkler, B., Ecker, W., and Gänser, H.P. (2018). A microstructural based creep model applied to alloy 718. Int. J. Plast. *105*, 62–73.

18. Lefebvre, W., Masquelier, N., Houard, J., Patte, R., and Zapolsky, H. (2014). Tracking the path of dislocations across ordered Al3Zr nano-precipitates in three dimensions. Scr. Mater. *70*, 43–46.

19. Choudhuri, D., Srinivasan, S.G., Gibson, M.A., Zheng, Y., Jaeger, D.L., Fraser, H.L., and Banerjee, R. (2017). Exceptional increase in the creep life of magnesium rare-earth alloys due to localized bond stiffening. Nat. Commun. *8*, 2000.

20. Singh, A.R.P., Nag, S., Chattopadhyay, S., Ren, Y., Tiley, J., Viswanathan, G.B., and Banerjee, R. (2013). Mechanisms related to different generations of γ′ precipitation during continuous cooling of a nickel base superalloy. Acta Mater. *61*, 280–293.

21. Knipling, K.E., Dunand, D.C., and Seidman, D.N. (2008). Precipitation evolution in Al-Zr and Al-Zr-Ti alloys during isothermal aging at 375-425 °C. Acta Mater. *56*, 114–127.

22. Nan, C.W., and Clarke, D.R. (1996). The influence of particle size and particle fracture on the elastic/plastic deformation of metal matrix composites. Acta Mater. *44*, 3801–3811.

23. De Lamaestre, R.E., and Bernas, H. (2006). Significance of lognormal nanocrystal size distributions. Phys. Rev. B Condens. Matter Mater. Phys. *73*, 125317.

24. Bai, Z., and Fan, Y. (2018). Abnormal strain rate sensitivity driven by a unit dislocation-obstacle interaction in BCC Fe. Phys. Rev. Lett. *120*, 125504.

25. Zhao, J., Gong, J., Saboo, A., Dunand, D.C., and Olson, G.B. (2018). Dislocation-based modeling of long-term creep behaviors of Grade 91 steels. Acta Mater. *149*, 19–28.

26. Kabir, M., Lau, T.T., Rodney, D., Yip, S., and Van Vliet, K.J. (2010). Predicting dislocation climb and creep from explicit atomistic details. Phys. Rev. Lett. *105*, 095501.

27. Kvapilova, M., Dvorak, J., Kral, P., Hrbacek, K., and Sklenicka, V. (2019). Creep behaviour and life assessment of a cast nickel–base superalloy MAR-M247. High Temp. Mater. Process. *38*, 590–600.

28. Yamamoto, Y., Brady, M.P., Lu, Z.P., Maziasz, P.J., Liu, C.T., Pint, B.A., More, K.L., Meyer, H.M., and Payzant, E.A. (2007). Creep-resistant, Al2O3-forming austenitic stainless steels. Science *316*, 433–436.